Thermal Management System for an Electric Machine with Additively Manufactured Hollow Conductors with Integrated Heat Pipes

Preprint

Towhid Chowdhury,[1] Salar Koushan,[1] Ali Al-Qarni,[1] A. El-Refaie,[1] Kevin Bennion,[2] Emily Cousineau,[2] Xuhui Feng,[2] and Bidzina Kekelia[2]

1 Marquette University
2 National Renewable Energy Laboratory

Presented at the International Conference on Electrical Machines (ICEM)
Valencia, Spain
September 5-8, 2022

NREL is a national laboratory of the U.S. Department of Energy
Office of Energy Efficiency & Renewable Energy
Operated by the Alliance for Sustainable Energy, LLC

This report is available at no cost from the National Renewable Energy Laboratory (NREL) at www.nrel.gov/publications.

Contract No. DE-AC36-08GO28308

Conference Paper
NREL/CP-5400-82597
November 2022

Thermal Management System for an Electric Machine with Additively Manufactured Hollow Conductors with Integrated Heat Pipes

Preprint

Towhid Chowdhury,[1] Salar Koushan,[1] Ali Al-Qarni,[1] A. El-Refaie,[1] Kevin Bennion,[2] Emily Cousineau,[2] Xuhui Feng,[2] and Bidzina Kekelia[2]

1 Marquette University
2 National Renewable Energy Laboratory

Suggested Citation
Chowdhury, Towhid, Salar Koushan, Ali Al-Qarni, A. El-Refaie, Kevin Bennion, Emily Cousineau, Xuhui Feng, and Bidzina Kekelia. 2022. *Thermal Management System for an Electric Machine with Additively Manufactured Hollow Conductors with Integrated Heat Pipes: Preprint*. Golden, CO: National Renewable Energy Laboratory. NREL/CP-5400-82597. https://www.nrel.gov/docs/fy23osti/82597.pdf.

NREL is a national laboratory of the U.S. Department of Energy
Office of Energy Efficiency & Renewable Energy
Operated by the Alliance for Sustainable Energy, LLC

This report is available at no cost from the National Renewable Energy Laboratory (NREL) at www.nrel.gov/publications.

Contract No. DE-AC36-08GO28308

Conference Paper
NREL/CP-5400-82597
November 2022

National Renewable Energy Laboratory
15013 Denver West Parkway
Golden, CO 80401
303-275-3000 • www.nrel.gov

NOTICE

This work was authored in part by the National Renewable Energy Laboratory, operated by Alliance for Sustainable Energy, LLC, for the U.S. Department of Energy (DOE) under Contract No. DE-AC36-08GO28308. Funded in part by the U.S. Department of Energy Office of Energy Advanced Research Projects Agency - Energy (ARPA-E) under Award Number DE-AR0001352. The views expressed herein do not necessarily represent the views of the DOE or the U.S. Government. The U.S. Government retains and the publisher, by accepting the article for publication, acknowledges that the U.S. Government retains a nonexclusive, paid-up, irrevocable, worldwide license to publish or reproduce the published form of this work, or allow others to do so, for U.S. Government purposes.

Cover Photos by Dennis Schroeder: (clockwise, left to right) NREL 51934, NREL 45897, NREL 42160, NREL 45891, NREL 48097, NREL 46526.

Thermal Management System for an Electric Machine with Additively Manufactured Hollow Conductors with Integrated Heat Pipes

T. Chowdhury, S. Koushan, A. Al-Qarni, A. EL-Refaie, K. Bennion, E. Cousineau, X. Feng, B. Kekelia

***Abstract* -- This paper discusses steps taken to size a thermal management system for an aircraft propulsion electric machine containing additively manufactured coils integrated with heat pipes aimed at boosting its specific power. Experimental setups are used to size and characterize heat pipes for the application and 3D thermal FEA is used to determine optimum heat transfer coefficient of convective boundaries. Geometric details of fin-based surface area enhancement required to reach target combined overall heat transfer coefficient (U) and surface area (A) performance (UA) in W/K, is worked out for relevant boundaries and the resulting UA is verified in 3D thermal FEA. Thermal management system's UA (by extension specific power) sensitivity to coolant temperature is explored and temperature distribution plots of optimized machine components are presented and discussed.**

***Index Terms*-- Specific Power (SP), Additive Manufacturing (AM), Electric Machines, Heat Pipes, Thermal Management System (TMS)**

I. Introduction

INCREASING climate change concerns in the past two decades have resulted in a push to develop technologies to reduce greenhouse gas (GHG) emissions contributed by the air transportation sector [1]–[4]. One solution to this need is to transition from fossil fuel-based propulsion engines to hybrid or electric propulsion enabled by electric motors driving propellers. State-of-the-art (SOTA) aircraft propulsion electric motors rated at power levels greater than 100 kW have system specific power (SP) range from 4.4 to 7.9 kW/kg [5]. This range is competitive to traditional turboprop engine system SP that roughly hovers around 3.4 to 5.3 kW/kg [6]–[8] but falls significantly shy of typical jet engine system SP of around 30.6 kW/kg [9].

As a result, the U.S. Department of Energy represented by ARPA-E has established a wide research opportunity funding for U.S. universities and companies to develop advanced electric aircraft propulsion technology under the ASCEND Program [1]. The technology is targeting to power a narrow body civilian series-hybrid electric aircraft with an electrical energy storage system and a turbine engine coupled to a generator feeding electrical power to the propulsion motors as shown in Fig. 1. Propulsion motor electromagnetic and system level specifications reflected in Table I and Fig. 2 were set to compete against conventional turbo jet engines. Additionally, target system SP in Table I is set to exceed current SOTA electric motors by a factor of two or greater. Consequently, this is a challenge from a thermal management system (TMS) standpoint as temperatures in the stator windings would exceed electrical insulation thermal limits under conventional TMS due to increased loss density resulting from higher system SP target.

Several techniques have been explored in the industry to extract heat from the stator. Some ideas involve only having a liquid cooled cooling jacket placed over the stator core

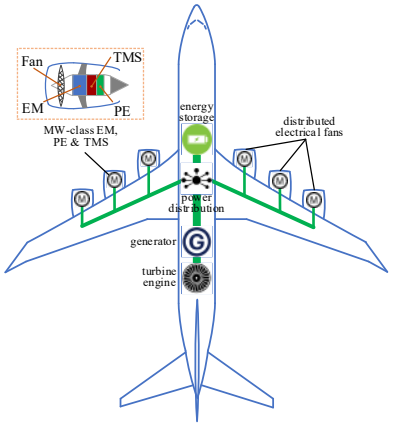

Fig. 1. Narrow-body civilian series-hybrid electric aircraft [24]

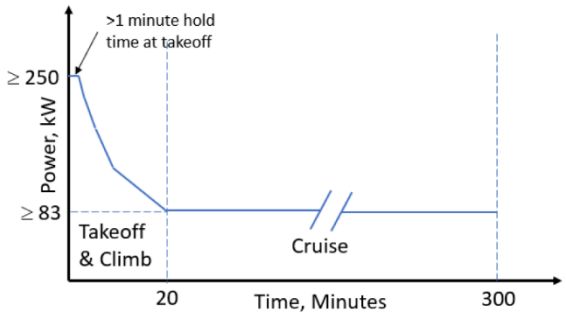

Fig. 2. Takeoff and cruise power-time curve [24]

TABLE I
DESIGN SPECIFICATIONS AND PARAMETERS

Item	Value
Machine SP	20 kW/kg
Machine Efficiency	>95%
System SP	>12 kW/kg
Peak Power	250 kW
Continuous Power	83 kW

The information, data, or work presented herein was funded in part by the Advanced Research Projects Agency-Energy (ARPA-E), U.S. Department of Energy, under Award Number DE-AR0001352.

T. Chowdhury, S. Koushan, A. Al-Qarni, A. M. EL-Refaie, are with the Werner Renewable Energy Lab, Department of Electrical and Computer Engineering, Opus College of Engineering, Marquette University, Milwaukee, WI 53233, USA (e-mails: towhid.chowdhury@marquette.edu; salar.koushan@marquette.edu; ali.alqarni@marquette.edu; ayman.el-refaie@marquette.edu).

K. Bennion, E. Cousineau, X. Feng, B. Kekelia, are with the Advanced Power Electronics and Electric Machines (APEEM) group at the National Renewable Energy Laboratory, Golden, CO 80401, USA (e-mails: kevin.bennion@nrel.gov; emily.cousineau@nrel.gov; xuhui.feng@nrel.gov; bidzina.kekelia@nrel.gov)

[10], [11] while others pair the stator cooling jacket with spray cooling of end winding [12], [13] or pursue spray cooling option all by itself [14], [15]. Other ideas explore extracting heat from further within the machine like having cooling channels at different locations within the stator slot [16]–[18]. One novel electric machine heat extraction idea patented is the use of heat pipes in [19]. [20] and [21] investigate using heat pipes in end windings and stator back iron respectively while [22] explores implementing heat pipes within the stator slot.

At Marquette University, a unique motor plus TMS design has been proposed in [23] to achieve the demanding specifications in Fig. 2. The proposed TMS design is for a surface mounted permanent magnet electric motor configured in Halbach array with fractional slot concentrated windings. This design features several key novelties which are (i) modular aluminum alloy ($AlSi_{10}Mg$) hollow additively manufactured (AM) coils (ii) modular power electronics (PE), and (iii) embedding of heat pipes into hollow AM coils and PE for cooling. The design proposed in [23] has been optimized to achieve an active SP and overall efficiency around 23 kW/kg and 92%, respectively, both of which exceed the current SOTA motors.

This paper furthers the work done in [23] by maturing the proposed TMS design through heat pipe testing and thermal modeling. The paper starts with discussing the machine loss breakdown and how this influences the final machine geometry. This is followed up with experimental characterization of the heat pipes and how this is implemented into the 3D FEA thermal model discussed in detail. Next, convective boundary heat transfer coefficients are explored for both the stator and rotor sections. Lastly, UA (by extension specific power) sensitivity to coolant inlet temperature is presented and temperature profile results for 40°C air coolant inlet temperature is presented and discussed.

II. Machine Loss Breakdown And Sizing Constraint

Loss breakdown for the machine is calculated using an electromagnetic finite element analysis (FEA) ANSYS model assuming a uniform machine temperature of 150°C as shown in Table II. These losses are for a 20° slice of the machine since it has a 1/18 symmetry as shown in Fig. 3.

Two factors were considered when sizing this machine along with its integrated TMS. Firstly, a heat pipe's maximum heat extraction capability (Q_{max}) increases with its cross-sectional area [25]; and secondly, for a fixed output power, the machine tends towards higher specific power with a decrease in machine outer diameter. As a result, for an optimized solution with high specific power, the stator space had to be negotiated between the stator core, the AM coil, and the heat pipes.

Furthermore, the conductor loss distribution of AM coil in Table III reflects that loss decreases as we go from layer 1 (closest to air gap) to layer 6 (furthest away from air gap). Note that this loss distribution doesn't account for losses in the end turns. Because we are assuming the same heat pipe and conductor cross-section geometry across all AM coil

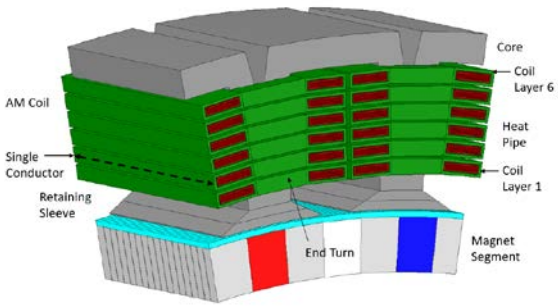

Fig. 3. 1/18 symmetry of machine

TABLE II
Loss Breakdown in 1/18 of the Machine

Loss Component	Loss [W]
AM Coil	794
Stator Core	277
Heat Pipes	94.5
Magnets	36.7
Friction & Windage	68

TABLE III
Loss Distribution of AM Coil per Conductor (Coil Side)

Layer #	Loss [W]
1	48
2	33
3	26
4	22
5	20
6	19

layers, the loss in layer 1 dictates the overall machine geometry. Our initial design [23], which was later found to not be sufficient from a TMS standpoint, was based on a flattened ⌀3 mm heat pipe tested to have a Q_{max} of 29 W.

This design was then revised to accommodate flattened ⌀6 mm heat pipe tested to have a Q_{max} of 67 W. The ⌀6 mm heat pipe's heat carrying capacity is 25% greater than 48 W loss per conductor generated in layer 1 per best practices followed when sizing heat pipes [26].

III. Heat Pipe Characterization and Thermal Model

A. Q_{max} and Contact Resistance Measurement

Q_{max} of the flattened ⌀3 mm and ⌀6 mm heat pipes were established using the test setup shown in Fig. 4. The condenser inlet fluid temperature was held at 80°C and the heat pipe evaporator section was heated using a current carrying wire wrapped around it. A thin layer of Kapton tape was applied between the heat pipe and the wire for electrical insulation. To determine Q_{max} of the heat pipe, power input to the evaporator was increased incrementally until the evaporator temperature either reached dry out or reached an upper temperature limit of 180°C. A thin layer of Kapton tape was used again to electrically insulate the wire from thermocouples mounted to monitor the evaporator temperature. Observing Fig. 5, the flattened ⌀6 mm heat pipe was found to have a Q_{max} of 67 W at a temperature limit of 180°C.

Thermal contact resistance (TCR) between the heat pipe and the AM coil under dry contact condition, is modeled in FEA based on data from test setup shown in Fig. 6. The heat pipe is inserted 1 cm into the AM coil resulting in a contact

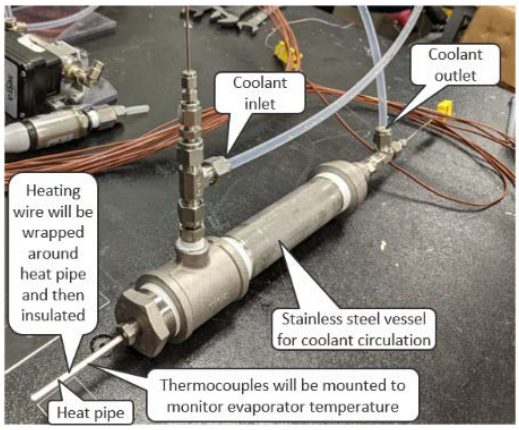

Fig. 4. Heat pipe Qmax testing setup

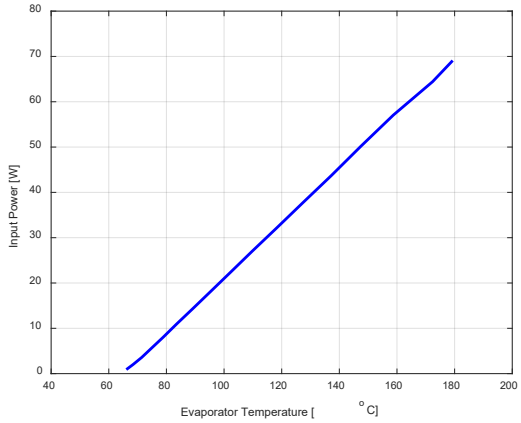

Fig. 5. Flattened ⌀6 mm heat pipe test results

area (A_C) of 93.3 mm^2. As before, heating wire is used to inject a known quantity of heat, Q (3.53 W), into the evaporator section resulting in a temperature difference between thermocouples 1 and 2 (ΔT) of 51.3ºC. TCR in mm^2·K/W is calculated using (2) to be 1358 mm^2·K/W.

$$TCR = \frac{A_C * \Delta T}{Q} \quad (2)$$

A 3D thermal FEA model representing test conditions was simulated and the predicted temperature profile of the AM coil is reflected in Fig. 7. To match ΔT between the test setup and FEA results, a correction factor of 1.325 was applied to the experimental TCR value resulting in a TCR of 1800 mm^2·K/W from FEA. Likewise, FEA TCR was also determined for two other interface materials, boron nitride and DOW TC 5622 thermal paste to be 514 mm^2·K/W and 170 mm^2·K/W respectively.

B. Thermal Model Setup

The 3D FEA thermal model representing 1/18 symmetry of the machine is shown in Fig. 8. The stator thermal model has a cooling jacket over the stator core and a convective boundary 'A' is applied over this cooling jacket. A dry press fit is assumed at the interface 'R2' between the core outer diameter and the cooling jacket resulting in a TCR of 167 mm^2·K/W per [27].

Heat pipes are extended from the AM coil to accommodate a convective boundary 'B'. DOW TC 5622 thermal paste interface is assumed between the heat pipe and

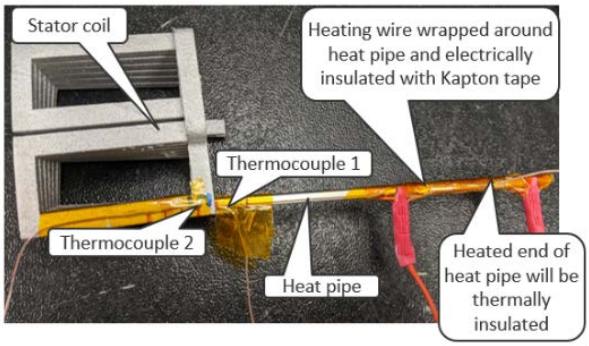

Fig. 6. Heat pipe contact resistance test setup

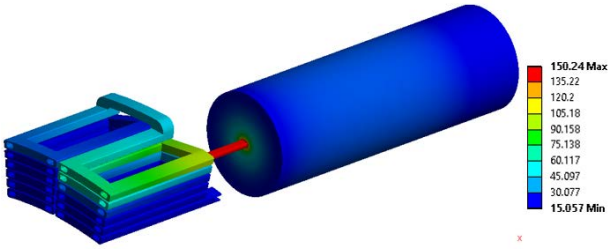

Fig. 7. Heat pipe contact resistance thermal FEA model

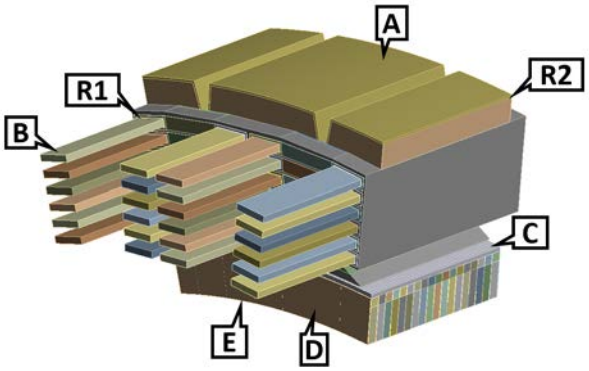

Fig. 8. Contact resistance and convective surfaces in the thermal model.

the AM coil 'R1' resulting in a TCR of 170 mm^2·K/W based on test data. TCR values were assumed for other contacts that include AM coil to turn insulation contact, turn insulation to ground insulation contact, ground insulation to core contact and ground insulation to coil contact.

The rotor is modeled as having three convective boundaries as shown in Fig. 8. 'C' is the convective boundary at the retaining sleeve outer diameter, 'D' is the convective boundary at the axial ends of the rotor, and 'E' is the convective boundary at the magnet inner diameter. A thin layer of epoxy insulation is present at the axial ends of the rotor and in between magnet segments in the axial direction only. TCR values were assumed for retaining sleeve to magnet contact, magnet to magnet contact, magnet to epoxy insulation contact and retaining sleeve to epoxy insulation contact.

Heat is generated within the thermal model by transferring AM coil loss, core loss, heat pipe loss and magnet loss in Table II from the electromagnetics FEA to the thermal FEA. Information on the regional break down of the different loss types is also captured in the thermal FEA. An overview of how the generated heat dissipates in the thermal model is described below. Losses in the stator are isolated from the rotor since the air gap is modeled as a thermal insulator.

Additionally, due to the presence of turn and ground insulation between the AM coil and the core, core losses predominantly dissipate through cooling jacket convective boundary 'A' and AM coil losses mostly escape through heat pipe convective boundary 'B'. Lastly, magnet losses dissipate through rotor convective boundaries 'C', 'D' and 'E'. All other surfaces not defined above are modeled to have an adiabatic convective boundary. Table IV summarizes thermal conductivities, λ, assumed for all materials in the thermal model. Note that λ of the flattened ⌀6 mm heat pipe was determined to be 15,000 W/m·K based on Celsia's heat pipe calculator tool [28].

IV. Heat Transfer Coefficients of Convective Boundaries

A. Stator Heat Transfer Coefficients

Stator convective boundaries, 'A' representing the cooling jacket and 'B' representing the heat pipes, require surface area enhancement through fins as shown in Fig. 9. Sizing analysis for these two convective boundaries is based on an iterative process that involves the following steps. First the thermal FEA model is run to estimate a convection heat transfer coefficient (H) value for each boundary assuming a coolant temperature of 40°C such that the maximum temperature of the system does not exceed an initial assumed temperature. Next, UA is calculated based on finless convective surface area in the 3D FEA thermal model for each boundary. Design details of the heat exchanger geometries to meet or exceed the target UA and other operating constraints within the context of a specific thermal management system layout are then worked out using the Engineering Equation Solver (EES) tool which references [29]. For both boundaries, H was calculated using heat transfer correlations (from EES) for flow through a rectangular duct.

The H value determined for each boundary is then combined with the overall surface area, fin efficiency, and surface efficiency to determine the effective UA based on heat exchanger equations from [30]. The resulting UA estimates for the two convective boundaries are then applied back to the 3D FEA thermal model by updating the H values in the software. The 3D FEA thermal model is then run to verify that the criterion discussed earlier is not violated. Lastly, the maximum temperature criterion for the 3D thermal FEA model is updated to reflect a value closer to the desired maximum temperature of the system (155°C) and the analysis steps are repeated.

For convective boundary 'A', the cooling jacket surface is modeled in EES as a surface cooler with a finned cooling duct extending into the airflow duct. Fin number and spacing were optimized to minimize fin mass while still meeting or exceeding the cooling jacket target UA. Air is assumed to be flowing axially at Mach 0.4 with static pressure of 83 kPa and inlet temperature of 40°C over the motor. For convective boundary 'B', air flow is assumed to be in the circumferential direction through a rectangular duct and will be flowing in between the radially placed heat pipes at a mass flow rate of 0.026 kg/s for each group of 12 heat pipes. Fins are axially stacked on to the heat pipes to increase the surface area available for cooling and fin number and spacing were optimized such that air pressure drop does not exceed 750 Pa to ensure compatibility with fan performance. Air temperature is assumed to be 40°C with static pressure of 83 kPa for boundary 'B'. The final value of H and UA for convective boundary 'A' and 'B' is listed in Table V.

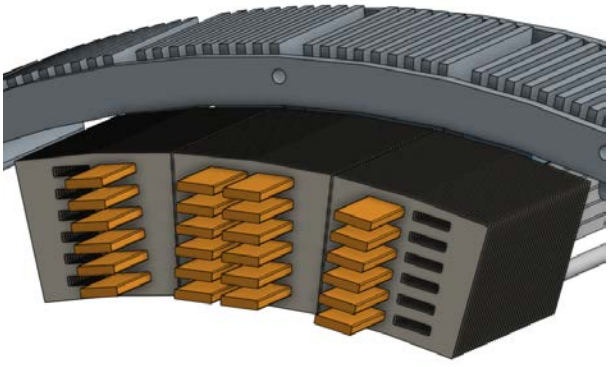

Fig. 9. Heat pipe and cooling jacket fins

TABLE IV
Thermal Conductivity of Materials

Part	Material	λ (W/m·K)
Cooling Jacket	Aluminum 6061	237.5
Stator Core (x,y,z)	Vacoflux 48	33, 33, 1.4
AM Coil	AlSi10Mg	103
Heat pipe	Copper-Water	15,000
Magnet	Recoma 35E	10
Retaining Sleeve	CF IM7/Peek	0.5
Turn Insulation	Kapton MT	0.75
Ground Insulation	Varnish	0.2
Magnet Insulation	Epoxy	0.25

B. Rotor Heat Transfer Coefficients

For the rotor thermal model, convective heat transfer coefficient, H, for boundaries 'C' and 'D' are estimated to be 139 W/m^2·K based on a 5000 RPM rotational velocity. This is a conservative value since it doesn't account for forced air flow over these boundaries. In contrast to boundaries 'C' and 'D', an equivalent H was calculated for convective boundary 'E'. This is because in practice the magnet will be resting over a rotor hub. The magnets are assumed to be sitting on a 6.5 mm thick titanium segment having a λ of 6.7 W/m·K and a 0.1 mm thick layer of epoxy having a λ of 0.3 W/m·K is assumed to be sandwiched between the magnet and the titanium segment. Additionally, TCR values were assumed for magnet to epoxy contact and epoxy to titanium contact. The λ and TCR values were then combined to determine an effective H value of 114 W/m^2·K for convective boundary 'E'. Value of H and UA for convective boundary 'C', 'D' and 'E' are listed in Table V.

TABLE V
Heat Transfer Coefficient at Convective Boundaries

Boundary	Name	H [W/m^2·K]	UA [W/K]
A	Cooling Jacket	1915	7.9
B	Heat Pipe Condenser	1649	21.8
C	Rotor Axial Ends	139	0.175
D	Sleeve Outer ⌀	139	0.323
E	Magnet Inner ⌀	114	0.247

V. Results and Discussion

A. Thermal Conductivity Sensitivity

Fig. 10 and 11 show results from sensitivity analysis carried out to observe how UA requirement for convective boundary changes with air inlet temperature for boundary 'A' and 'B' respectively for the full motor. For both boundary cases one curve is plotted for maximum temperature of 150°C and another curve is plotted for maximum temperature of 160°C. Observing Fig. 10 and 11, UA requirement of the boundaries start to increase significantly with each °C rise for temperatures beyond 60°C resulting in lower specific power (W/kg) of the TMS. This is because the fin surface area required increases with increasing UA for an assumed H value.

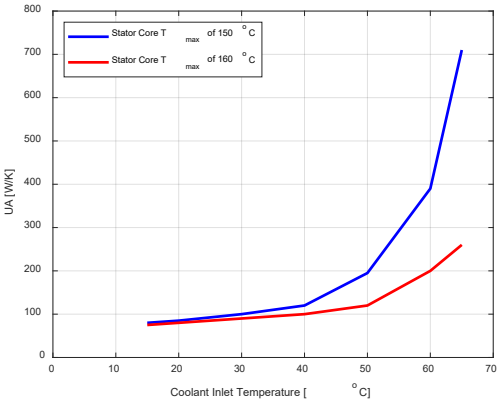

Fig. 10. Sensitivity of convective boundary 'A' for full motor

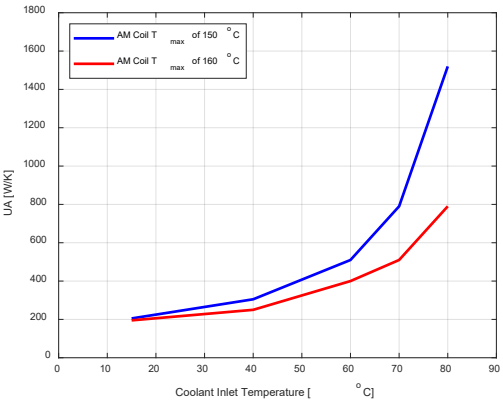

Fig. 11. Sensitivity of convective boundary 'B' for full motor

B. Stator Temperature Profile

Resulting temperature profiles of the heat pipes, AM coil and stator core, are shown in Fig. 12-14. The following observation have been made

- For all components the peak temperature does not exceed the target of 155°C as desired.
- Average temperature of the AM coil conductor decreases as we go from layer 1 to layer 6. This trend is expected as the losses per conductor also decreases.
- Maximum temperature is observed at the end turn of the AM coil for each layer since heat pipes are not directly cooling this region.
- Temperature in the stator core decreases going from inner to outer diameter as most heat escapes through the outer diameter

C. Rotor Temperature Profile

Rotor temperature profile shown in Fig. 15 is a result of assuming a conservative H value of 100 W/m^2·K for all three convective boundaries 'C', 'D' and 'E' and an air inlet temperature of 40°C. Under these assumptions the maximum temperature of the rotor is 121°C. However, the TMS system is setup such that the air first cools the heat pipes before it cools the rotor. As a result, actual air inlet temperature to the rotor is close to 57°C. Hence, the resulting maximum temperature of the rotor will be 138°C which is below the target temperature of 155°C. Notice from Fig. 15 that the temperature of the magnet is higher towards the outer radius. This is because eddy current losses in the magnet are also concentrated towards the outer radius.

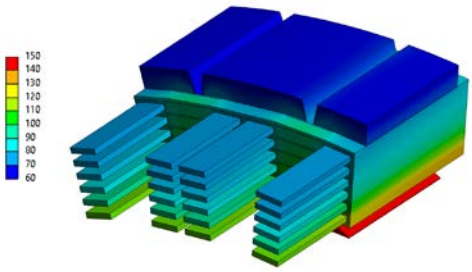

Fig. 12. System temperature distribution

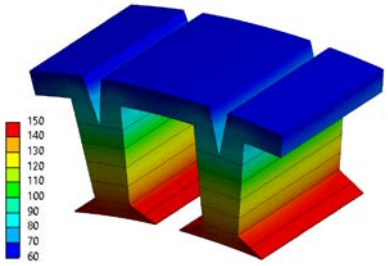

Fig. 13. Stator core temperature distribution

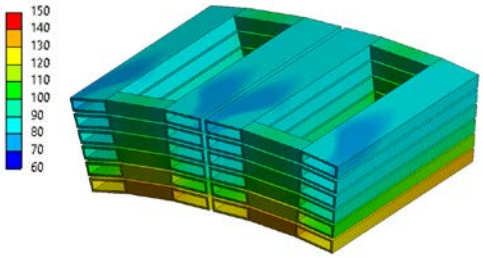

Fig. 14. AM Coil temperature distribution

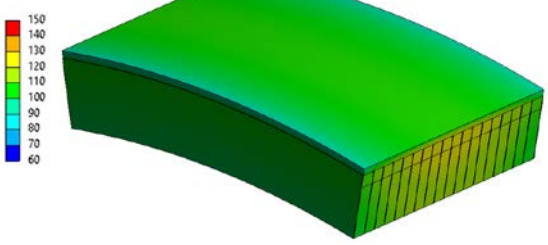

Fig. 15. Magnet and retaining sleeve temperature distribution

VI. Conclusion

This paper has successfully discussed steps taken to size a thermal management system for a surface permanent magnet machine featuring additively manufactured coils integrated with heat pipes. The system takes into consideration loss distributions in the AM coil, stator core, magnets, and heat pipes themselves. Heat pipe for the machine was sized based on comparing its experimentally determined Q_{max} to the maximum heat generated per AM Coil conductor (coil side). TCR between the heat pipe and the AM coil was experimentally determined and a FEA correction factor was adopted for thermal simulations. A complete 3D FEA thermal model of the machine was created taking into consideration λ of materials and TCR of interfaces. This model was then used to determine optimum heat transfer coefficient for all convective surfaces based on system target temperature.

It was realized that the cooling jacket and heat pipe convective boundaries required surface area enhancement through fins. Target combined overall heat transfer coefficient (U) and surface area (A) performance (UA) in W/K, for these two boundaries were determined and finned geometries were designed to meet or exceed the target UA and meet other operating constraints using the Engineering Equation Solver tool. The finalized geometry resulted in an active specific power of 23.8 kW/kg, active specific power including TMS of 19.5 kW/kg, system specific power of 10.1 kW/kg and efficiency of 91.8%. The system specific power value excludes the mass of shaft, housing and bearings since they are counted as part of the plane structure but includes mass of the rotor hub, magnets, stator, power electronics and the thermal management system. Additionally, this design falls short of target efficiency (> 95%) as pushing for high specific power accompanies a tradeoff of lower efficiency. Lastly, temperature profiles of all the components are presented and discussed.

VII. Acknowledgment

We would like to acknowledge the thermal testing and analysis work done by the Advanced Power Electronics and Electric Machines (APEEM) team at the National Renewable Energy Laboratory in support of this project.

The information, data, or work presented herein was funded in part by the Advanced Research Projects Agency-Energy (ARPA-E), U.S. Department of Energy, under Award Number DE-AR0001352. The views and opinions of authors expressed herein do not necessarily state or reflect those of the United States Government or any agency thereof.

VIII. References

[1] https://arpa-e.energy.gov/technologies/programs/ascend

[2] https://www.energy.gov/articles/department-energy-announces-55-million-funding-electric-aviation-programs

[3] https://www.energy.gov/articles/department-energy-announces-33-million-funding-carbon-neutral-hybrid-electric-aviation

[4] https://www.nasa.gov/press-release/nasa-issues-contracts-to-mature-electrified-aircraft-propulsion-technologies

[5] A. El-Refaie and M. Osama, "High specific power electrical machines: A system perspective," 2017 20th International Conference on Electrical Machines and Systems (ICEMS), 2017, pp. 1-6, doi: 10.1109/ICEMS.2017.8055931.

[6] https://www.easa.europa.eu/sites/default/files/dfu/TCDS%20PW150%20series%20issue%2001_20141119_1.0.pdf

[7] https://rgl.faa.gov/Regulatory_and_Guidance_Library/rgMakeModel.nsf/0/958b10612fcd574f86258211006d4706/$FILE/TE1CH_Rev%2032.pdf

[8] Haas, D. W. (1996). The instrumentation design and control of a T63-A-700 gas turbine engine (thesis). Naval Postgraduate School, Monterey, CA.

[9] https://ntrs.nasa.gov/api/citations/20090004620/downloads/20090004620.pdf

[10] L. Cuiping, G. Zhengwei, L. Junhui, Z. Bing and D. Xiucui, "Optimal design of cooling system for water cooling motor used for mini electric vehicle," 2017 20th International Conference on Electrical Machines and Systems (ICEMS), 2017, pp. 1-4, doi: 10.1109/ICEMS.2017.8056319.

[11] Z. Huang, S. Nategh, V. Lassila, M. Alaküla and J. Yuan, "Direct oil cooling of traction motors in hybrid drives," 2012 IEEE International Electric Vehicle Conference, 2012, pp. 1-8, doi: 10.1109/IEVC.2012.6183163.

[12] L. Ye, F. Tao, L. Qi and W. Xuhui, "Experimental investigation on heat transfer of directly-oil-cooled permanent magnet motor," 2016 19th International Conference on Electrical Machines and Systems (ICEMS), 2016, pp. 1-4.

[13] A. M. EL-Refaie et al., "Advanced High-Power-Density Interior Permanent Magnet Motor for Traction Applications," in IEEE Transactions on Industry Applications, vol. 50, no. 5, pp. 3235-3248, Sept.-Oct. 2014, doi: 10.1109/TIA.2014.2305804.

[14] L. Zhenguo, R. Lin and T. Longyao, "Heat transfer characteristics of spray evaporative cooling system for large electrical machines," 2015 18th International Conference on Electrical Machines and Systems (ICEMS), 2015, pp. 1740-1743, doi: 10.1109/ICEMS.2015.7385321.

[15] C. Liu et al., "Experimental Investigation on Oil Spray Cooling With Hairpin Windings," in IEEE Transactions on Industrial Electronics, vol. 67, no. 9, pp. 7343-7353, Sept. 2020, doi: 10.1109/TIE.2019.2942563.

[16] G. Venturini, G. Volpe and M. Popescu, "Slot Water Jacket Cooling System for Traction Electrical Machines with Hairpin Windings: Analysis and Comparison," 2021 IEEE International Electric Machines & Drives Conference (IEMDC), 2021, pp. 1-6, doi: 10.1109/IEMDC47953.2021.9449581.

[17] W. Sixel, M. Liu, G. Nellis and B. Sarlioglu, "Ceramic 3-D Printed Direct Winding Heat Exchangers for Thermal Management of Concentrated Winding Electric Machines," in IEEE Transactions on Industry Applications, vol. 57, no. 6, pp. 5829-5840, Nov.-Dec. 2021, doi: 10.1109/TIA.2021.3104273.

[18] A. Acquaviva, S. Skoog and T. Thiringer, "Design and Verification of In-Slot Oil-Cooled Tooth Coil Winding PM Machine for Traction Application," in IEEE Transactions on Industrial Electronics, vol. 68, no. 5, pp. 3719-3727, May 2021, doi: 10.1109/TIE.2020.2985009.

[19] T. Hasset and M. Hodowanec, "Electric motor with heat pipes," U.S. Patent 7 569 955 B2, 2009.

[20] Y. Guo and A. Wang, "Thermal Design and Simulation of winding cooling for permanent magnet synchronous motor of electric vehicle," 2021 IEEE 4th Student Conference on Electric Machines and Systems (SCEMS), 2021, pp. 01-05, doi: 10.1109/SCEMS52239.2021.9646152.

[21] Z. Yu, Y. Li, Y. Jing and J. Wang, "Cooling System of Outer Rotor SPMSM for a Two-Seater All-Electric Aircraft Based on Heat Pipe Technology," in IEEE Transactions on Transportation Electrification, doi: 10.1109/TTE.2021.3127555.

[22] C. Dong, Y. Qian, Y. Zhang, X. Hu and W. Zhuge, "Coupled Thermal-Electromagnetic Parametric Modeling of Permanent Magnet Machine Based on Flat Heat Pipe Cooling," 2020 23rd International Conference on Electrical Machines and Systems (ICEMS), 2020, pp. 1689-1694, doi: 10.23919/ICEMS50442.2020.9291188.

[23] F. Wu, A. M. EL-Refaie and A. Al-Qarni, "Additively Manufactured Hollow Conductors Integrated With Heat Pipes: Design Tradeoffs and Hardware Demonstration," in IEEE Transactions on Industry Applications, vol. 57, no. 4, pp. 3632-3642, July-Aug. 2021, doi: 10.1109/TIA.2021.3076423.

[24] A. Al-Qarni, A. EL-Refaie and F. Wu, "Impact of Machine Parameters on The Design of High Specific Power Permanent Magnet Machines for Aerospace Applications," 2021 IEEE International Electric

Machines & Drives Conference (IEMDC), 2021, pp. 1-8, doi: 10.1109/IEMDC47953.2021.9449592.
[25] Zhang Y. Heat Pipes : Design, Applications and Technology. Nova Science Publishers, Inc.; 2018. Accessed March 28, 2022. https://search.ebscohost.com/login.aspx?direct=true&db=cat06952a&AN=mul.b3684425&site=eds-live&scope=site
[26] Zhang, Y. (2018) Heat pipes : design, applications and technology. Nova Science Publishers, Inc. (Mechanical engineering theory and applications).
[27] https://celsiainc.com/heat-sink-blog/heat-pipe-calculator-use-instructions/
[28] J. E. Cousineau, K. Bennion, V. Chieduko, R. Lall, and A. Gilbert, "Experimental Characterization and Modeling of Thermal Contact Resistance of Electric Machine Stator-to-Cooling Jacket Interface Under Interference Fit Loading," J. Thermal Sci. Eng. Appl, vol. 10, no. 4, May 2018.
[29] https://celsiainc.com/resources/calculators/heat-pipe-calculator/
[30] G. Nellis and S. Klein, Heat Transfer. Cambridge University Press, 2009.
[31] F. Incropera and D. DeWitt, Fundamentals of Heat and Mass Transfer, 4th ed. John Wiley & Sons, 1996.

IX. Biographies

Towhid Chowdhury received his Bachelor's degree in mechanical engineering from Virginia Tech, Blacksburg, VA, in Spring 2018. Post-graduation he worked as an electric motor design engineer for three years at InMotion US. He is currently pursuing a Master's degree in electrical engineering from Marquette University, Milwaukee, WI. His research interests are in the electromagnetic and mechanical design of electric machines.

Salar Koushan (S'18) received his B.Sc. in Electrical Engineering from the University of Tabriz, Tabriz, Iran, in 2014, and he got his M.Sc. from Middle East Technical University, Ankara, Turkey, In 2020. He started his Ph.D. at Marquette University in 2021. His research interests are the Design and Optimization of Electrical Machines, and Electromagnetic Analyses using FEA.

Ali Al-Qarni (S'21) received the B.Sc. degree in electrical engineering from King Khalid University, Abha, Saudi Arabia, in 2015, and the M.S. degree in electrical engineering from the Marquette University, Milwaukee, WI, USA, in 2020, where he is currently working towards his Ph.D. degree. His research interests include the analysis, design and optimization of magnetic gears, magnetically geared machines, advanced permanent-magnet machines, and ultra-fast actuators

Ayman M. EL-Refaie received the M.S. and Ph.D. degrees in electrical engineering from the University of Wisconsin-Madison in 2002 and 2005, respectively. Between 2005 and 2016 he has been a principal engineer and a project leader at the Electrical Machines and Drives Lab at General Electric Global Research Center. His research interests include electrical machines and drives. Since January 2017, he joined Marquette University as the Werner Endowed Chair for Energy Sustainability. He has over 160 journal and conference publications. He has 48 issued US patents.

At GE, he worked on several projects that involve the development of advanced electrical machines for various applications including aerospace, traction, wind, and water desalination. He was the chair for the IEEE IAS Transportation Systems committee and an associate editor for the Electric Machines committee. He was a technical program chair for the IEEE 2011 Energy Conversion Conference and Exposition (ECCE). He was the general chair for ECCE 2014 and 2015 ECCE steering committee chair. He was the general chair of IEMDC 2019. He is the past chair of the IEEE IAS Industrial Power Conversion Systems Department and currently he is the IEEE Industry Applications Society Publications Department chair.

Kevin Bennion is a member of the Advanced Power Electronics & Electric Machines team in the Transportation & Hydrogen Systems Center at the National Renewable Energy Laboratory (NREL). He leads research projects with DOE and industry focused on thermal management of power electronics and electric motors. He has also supported research projects related to high power charging, vehicle thermal management and vehicle systems analysis. Kevin came to NREL from Ford Motor Company where he worked on powertrain systems and controls including electric drive components for hybrid electric vehicles. Kevin holds a Master of Science from Rensselaer Polytechnic Institute and a Bachelor of Science from Brigham Young University, both in Mechanical Engineering.

Emily Cousineau is a Researcher on the Advanced Power Electronics and Electric Machines (APEEM) Team at National Renewable Energy Laboratory (NREL). Emily Develops computational models (analytical, FEA, and CFD utilizing commercial software) for prediction, comparison, and validation of systems. She also performs experimental thermal materials characterization specializing in small-sample size, low thermal conductivity materials, anisotropic and inhomogeneous materials, and thermal interfaces. Majority of work is in the context of electric machines and power electronics from a thermal management perspective. Emily holds a Master's and Bachelor's degree in engineering with a mechanical specialty from Colorado School of Mines.

Xuhui Feng joined CIMS in 2012 as a postdoctoral researcher supporting advanced power electronics and is a senior research engineer in Advanced Power Electronics and Electric Machines group. His primary duties involve performing modeling, testing, and analysis with a focus on power electronics and electric machine thermal management systems. Before coming to NREL, Feng was a research assistant at Iowa State University's Micro/Nanoscale Thermal Science Laboratory, where he conducted thermal characterization of one-dimensional micro/nanoscale materials using various transient techniques. He also served as a research assistant at the University of California's Renewable Energy Resources Laboratory and the University of Nebraska's Micro/Nanoscale Thermal Science Lab. He earned his Ph.D. in mechanical engineering from Iowa State University, his master's degree in mechanical engineering from the University of Nebraska, and his bachelor's degree in thermal science and energy engineering from the University of Science and Technology of China."

Bidzina Kekelia is a Senior Research Engineer in the Advanced Power Electronics and Electric Machines (APEEM) Group within the Center of Integrated Mobility Sciences at the NREL. He earned his Bachelor's (Hons) in Mechanical Engineering from Georgian Technical University (1992), M.S. in Renewable Energy (Solar Thermal & PV) from the University of Oldenburg (1999) and Ph.D. in Mechanical Engineering from the University of Utah (2012). After receiving his Ph.D., he worked as a postdoctoral research associate at the University of Utah, developing thermal battery prototypes for electric vehicles. Since joining NREL in 2015, Bidzina's research has focused on exploring novel cooling methods for power electronics and electric drives.